Preprints of the 19th World Congress
The International Federation of Automatic Control
Cape Town, South Africa. August 24-29, 2014

Online estimation of vehicle load and mass distribution for ground vehicles

S. Bottelli * **M. Tanelli** * **I. Boniolo** ** **S.M. Savaresi** *

* *S. Bottelli, M. Tanelli and S. M. Savaresi are with the Dipartimento di Elettronica, Informazione e Bioingegneria, Politecnico di Milano, Piazza Leonardo da Vinci 32, 20133 Milano, Italy.*
** *I. Boniolo is with the Dipartimento di Ingegneria, Università degli Studi di Bergamo, Via Marconi 14, Dalmine, Bergamo, Italy.*

Abstract: The vehicle mass and its distribution on the vehicle is an important information for several applications, from safety-oriented control systems to fleet management in public transport, courier services, garbage collection and so on. Specifically, an online estimation of such quantities must be provided and the results should be available relying on a minimum set of sensors, to reduce costs and possibly avoid an *ad-hoc* instrumentation. This paper proposes a frequency-based data processing scheme to address this issue, which relies on vertical acceleration and speed angular velocity measurements only. The validity of the approach is assessed both on simulations in a multibody environment and on experimental data.

1. INTRODUCTION

Knowledge of the vehicle mass is of utmost importance, especially when dealing with heavy-duty transportation systems. A wrong information about the load mass or its distribution along the vehicle or inside the trunk can lead to serious hazards to vehicle stability, or even to structure wreckage. Trucks axles are in fact subject to extremely large forces due to the heavy load of the vehicle, and fractures and cracks are very common consequences of load imbalance.

Moreover, nearly all commercial vehicles are equipped with active safety systems, whose electronic controllers are tuned based on a specific vehicle model, which in general comprises the mass information. Further, many fault detection and supervision methodologies rely on vehicle state observers, which are again tuned on the vehicle parameters, including mass and – possibly – additional load for heavy-duty vehicles, [Fathy et al., 2008, Vahidi et al., 2005].

Further, in the context of the so-called *smart cities*, automatic fleet management and logistics for commercial vehicles and for public services such as garbage collection must be designed so that an online optimization of the vehicles usage can be performed to optimize their exploitation and minimize the related energy consumption, [Stefansson and Lumsden, 2008]. In all these applications, the vehicle mass and/or the load distribution may vary with time, so that an online monitoring of such quantities must be made performed, possibly with a cheap and reduced sensor configuration.

To address this issue, two main types of approaches have been proposed so far: non-inertial and inertial methods. The former do not need inertial sensors for their operation, but rather employ suspensions-based systems equipped with stroke sensors, or pressure sensors, see *e.g.*, Lacuck [1971], Reichow et al. [1977]. The main advantage of these methods is the high precision of the sensor measurement, which in however due to a high costs equipment and calls for not trivial installation procedures. Inertial methods, on the contrary, make use of inertial sensors such as accelerometers or gyros, and they can provide rather reliable mass estimation with low cost and easy installations. Inertial methods can be further divided into approaches that rely either on a longitudinal or on a vertical dynamic description of the vehicle motion. Longitudinal dynamics based methods (*e.g.*, [Fathy et al., 2008], [Winstead and Kolmanovsky, 2005] and [Vahidi et al., 2005]) are typically developed from the basic form of Newton's law. The immediate consequence of this fact is that the longitudinal force applied to the vehicle must be known or somehow estimated. On the other hand, vertical dynamics based methods (*e.g.*, [Imine et al., 2006], [Rozyn and Zhang, 2010] and [Pence, 2011]) rely on the vertical filtering effect of the vehicle: the vertical excitation of the chassis is usually expressed as the output of a transfer function which is fed with ground vertical excitation or wheels vertical excitation, which of course need to be measured.

The approach proposed in this paper (which has been patented in [Savaresi et al., 2013]) follows conceptually the vertical dynamics framework, with the advantage of providing a reliable estimation of a vehicle load and of its distribution without the need of measuring neither road profile nor the wheel vertical motion, but simply by processing the vertical acceleration of the chassis and the pitch speed, the latter being required to provide additional information on the load distribution. The final performance of the method are expected to provide reliable means to discern among a finite set of loads and distributions (and not to detect mass variations of a few kilos in a whole vehicle), which is the precision needed to support the aforementioned applications.

The structure of the paper is as follows. Section 2 provides a description of the simulation and of the experimental setup considered in this work, together with the assumptions on the road description. Section 3 presents the proposed estimation algorithm, while Section 4 assesses its validity both in simulation and on experimental data.

2. VEHICLE AND ROAD DESCRIPTION

Before discussing the estimation algorithm, it is worth introducing the simulation tools and the experimental set up considered in this work.

Table 1. Vehicle parameters

Description	Value	Unit	Description	Value	Unit
Sprung mass	1240	kg	Unsprung mass	$4 \cdot 40$	kg
Height	1.8	m	Roll Inertia	486	kgm^2
Width	1.7	m	Pitch Inertia	2975	kgm^2
Length	3.5	m	Yaw Inertia	2975	kgm^2

2.1 Vehicle Model

Within the Carsim simulation environment, a full car model was defined. To employ a realistic vehicle description, the CarSim simulation environment was used. This is a full vehicle, multibody simulator, which comprises all the vehicle and tire dynamics. A small commercial vehicle was then employed to validate the proposed approach within an experimental setting. For the current application a small van vehicle model was selected, but the method can be readily applied to any other vehicle. The parameters of interest are listed in Table 1. A vertical accelerometer and a pitch gyro were added, integral to the vehicle chassis and positioned in the rear part of the trunk. The final vehicle model allowed us to load different masses in different positions inside the vehicle.

2.2 Road Profile

In order to correctly simulate the systems behavior, a realistic road profile has to be determined. To this end, the road description was defined (see [Rotenberg, 1972] for details) as the output of a dynamic system of the form

$$\begin{aligned} z_r(t) &= \frac{1}{s+\alpha_r v} u(t), \quad u(t) \sim WN \\ E[u(t)u(t-\tau)] &= 2\alpha_r v \sigma^2 \delta(\tau), \end{aligned} \tag{1}$$

where σ^2 is the variance of the road irregularities, α_r is a coefficient that depends on the shape of the road irregularities ($\alpha_r = 0.15$ for standard asphalt), v is the vehicle speed, $\delta(\tau)$ is the Dirac delta function and $E[\cdot]$ is the expectation operator. To model different road profiles, the International Roughness Index (IRI) standard [Paterson, 1986] is used. A road IRI is a dimensionless number which measures the road profile roughness: $IRI = 0$ implies a perfectly flat road, while higher IRI values refer to rougher road profiles. The IRI value is computed as

$$IRI = \frac{\int_0^{t_{end}} \left| z_{body}(t) - z_{wheel}(t) \right| dt}{L_r}, \tag{2}$$

obtained by simulating a given quarter car vehicle model (known as the Golden Car) which drives along the road profile at a constant speed of 80 km/h. The suspension deflection is evaluated and integrated over the road length L_r. The nominal value of σ^2 was chosen such that the resulting road has $IRI = 4$, which corresponds to an average maintained pavement.

2.3 Experimental Set Up

For experimental tests, a small commercial vehicle (FIAT Doblo') was used, quite close with the vehicle model used in the simulation. An inertial unit (with three accelerometers and three gyros) was installed on the vehicle, at the rear of the trunk. A GPS sensor was also present on the roof of the car. The available measurements were sampled at 50Hz.

3. MASS AND LOAD DISTRIBUTION ESTIMATION

In this section the proposed estimation algorithm, which will provide as output the estimated vehicle mass and the load distribution along the longitudinal axis, is presented. Specifically, the load distribution D is computed as the percentage amount of the vehicle load (including the vehicle mass) that insists on the front axle. Namely, one has

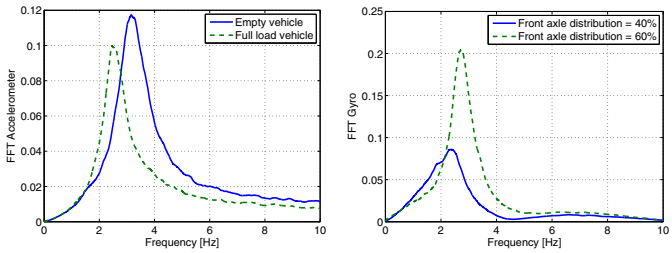

Fig. 1. Spectra of the vertical acceleration for different vehicle loads (left); Spectra of the pitch rate for different load distributions (right).

$$D = \frac{\frac{1}{2}M + (1 - \frac{d}{l})L}{M + L}, \tag{3}$$

where M is the vehicle mass, L is the vehicle load, d is the position of the vehicle load CoG along the vehicle longitudinal axis (measured from the front axle), and l is the vehicle wheelbase. The mass of the vehicle is supposed to have its CoG at $\frac{l}{2}$.

3.1 Main Idea

The estimation approach is based on the observation that the frequency spectrum of the both the vertical accelerometer and the pitch gyro significantly varies as a function of the vehicle load and its distribution. This can be appreciated by inspecting the left plot in Fig. 1, which depicts the accelerometer spectra obtained where the same vehicle is facing the same road profile, but with different loads, located in the same position inside the trunk. In the right plot of Fig. 1, instead, the results obtained for the pitch gyro spectra when the same vehicle is driven along the same road profile, with the same load but with different load distributions are depicted. As can be seen, both the magnitude of the maximum and its frequency location vary according to the different working conditions. Most interestingly, each of the two sensors captures one of the two aspects of interest: the accelerometer can be used to estimate the load, while the gyro to estimate its distribution. This means that if only one of the two is of interest for a specific application, a single sensor can be used.

To discriminate between the above differences in the spectra, the *ratio index* will be used. The aim of this quantity is to give a concise information about the *shape* of the signal spectrum. The differences between the spectra given by different loads (or by differently distributed loads) are located in some specific ranges of frequencies. Thus, by filtering the signal with a set of band pass filters it is possible to isolate the information contained in every specific range of frequencies. Then, by a suitable post processing of the filtered signals, the load and its distribution can be estimated. Specifically, the complete procedure can be summarized as follows:

- Find a set of frequency ranges in which the spectrum shape is *sensitive* to variations in the vehicle load and in its distribution, and design a dedicated band pass filter for each frequency range to be selected;
- Post process the filtered signals to compute the ratio index;
- Fit a static black box model to establish the relation between the ratio index and both load and load distribution.

Table 2. Frequency ranges selected for identification purposes

Frequency range	Center Frequency (f)	Width (w)
$a1$	2.4 Hz	0.05 Hz
$g1$	1.7 Hz	0.05 Hz
$a2$	3.25 Hz	0.05 Hz
$g2$	2.85 Hz	0.05 Hz

In what follows, each of these steps will be discussed.

3.2 Frequency-based data processing

As mentioned above, the first step is to isolate a frequency band in which the difference between the spectra obtained of different load or different load distributions is maximized. In what follows, the attention will be mainly focused on the vertical acceleration signal $\ddot{y}(t)$, but then it will be shown that the same procedure can be applied, identically, to the pitch rate signal $\dot{\psi}(t)$ for extracting information on the load distribution. For analysis purposes, the spectra obtained with a fully loaded vehicle will be compared to that obtained with an empty vehicle. To quantify the comparison between the two, the following cost function is introduced

$$J_L(f,w) = \int_{f-w/2}^{f+w/2} \frac{\Gamma_{fullload}(\omega) - \Gamma_{empty}(\omega)}{w} d\omega, \qquad (4)$$

in which the difference between the spectrum of the accelerometer data related to a fully loaded vehicle ($\Gamma_{fullload}(\omega)$) and an empty vehicle spectrum ($\Gamma_{empty}(\omega)$) is computed for different frequency ranges, defined by a center band frequency f and a bandwidth w. Each integral is then normalized with respect to its bandwidth. The maximum values of $|J_L(f,w)|$ represent the frequency ranges (defined by a center frequency f and a bandwidth w) in which the difference between the spectra is maximized. The same procedure is applied to the gyroscope data, in order to estimate the set of frequencies in which the signal spectrum is more sensitive to the load distribution inside the trunk. To this aim, the cost function J_D is computed as

$$J_D(f,w) = \int_{f-w/2}^{f+w/2} \frac{\Gamma_{60\%}(\omega) - \Gamma_{40\%}(\omega)}{w} d\omega, \qquad (5)$$

where $\Gamma_{60\%}$ is the spectrum of the gyroscope data related to a vehicle having a load distribution equal to 60%; similarly, $\Gamma_{40\%}$ is the spectrum of the gyroscope data related to a vehicle having load distribution equal to 40%.

After this analysis, the frequency ranges listed in Table 2 were selected as those maximizing the differences in the two spectra of interest.

Having defined the pairs (f_*, w_*) corresponding to which $|J_L(f,w)|$ and $|J_D(f,w)|$ are maximized, a band pass filter of the form

$$F_*(s) = 1 - \frac{s^2 + (2\pi f_*)^2}{s^2 + 2\pi w_* s + (2\pi f_*)^2} \qquad (6)$$

is designed for each frequency range. Finally, a concise dimensionless number must be extracted from the filtered signals to give a precise indication of the quantities of interest. To this end, the spectrum of each filtered signal is computed, and the The *ratio index* R_a (computed up to 10Hz) defined as

$$R_a = \frac{\int_0^{2\pi 10} \Gamma_{a1}(\omega) d\omega}{\int_0^{2\pi 10} \Gamma_{a2}(\omega) d\omega}, \qquad (7)$$

where $\Gamma_{a1}(\omega)$ is the spectrum of $F_{a1}(s)\ddot{Y}(s)$, and $\Gamma_{a2}(\omega)$ is the spectrum of $F_{a2}(s)\ddot{Y}(s)$.

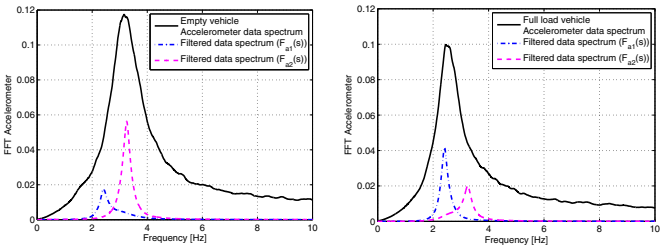

Fig. 2. Empty vehicle spectra (left); Full loaded vehicle spectra (right).

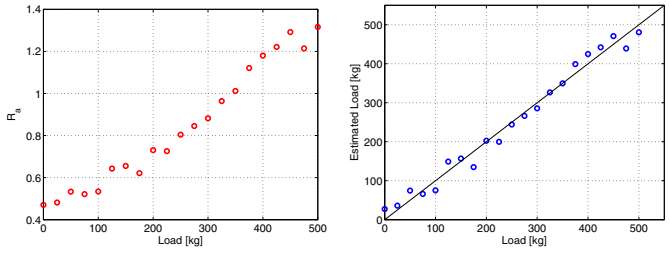

Fig. 3. Load estimation: ratio index of the acceleration spectrum (left); model fitting (right).

For example, Fig. 2 shows the difference between the ratio index of an empty vehicle and a full loaded one, when driven along the same road. Specifically, the spectrum of the accelerometer signal is represented, as well as the band pass filtered signals. The ratio index for empty vehicle is $R_a = 0.43$, while that of the full load vehicle $R_a = 1.33$.

Similarly, the ratio index related to the gyro signal R_g is computed (again up to 10 Hz) as

$$R_g = \frac{\int_0^{2\pi 10} \Gamma_{g1}(\omega) d\omega}{\int_0^{2\pi 10} \Gamma_{g2}(\omega) d\omega}, \qquad (8)$$

where $\Gamma_{g1}(\omega)$ is the spectrum of $F_{g1}(s)\dot{\psi}(s)$, and $\Gamma_{g2}(\omega)$ is the spectrum of $F_{g2}(s)\dot{\psi}(s)$. Finally a fitting problem must be solved to obtain the relationship between the ratio index R_a of the accelerometer spectrum and the load, and that of the pitch gyroscope (R_g) and the load distribution.

To study the relationship between R_a and the vehicle load a fixed load distribution was chosen for the front and the rear axles, positioning the load exactly at the vehicle CoG. Then, simulation experiments have been carried out with different loads (added to the empty vehicle), ranging from 0 kg to 450 kg.

In the left plot of Fig. 3, the values of R_a obtained for different vehicle loads are represented. After having normalized such values between -1 and 1 to improve the numerical precision of the fitting, different regressors were considered. An F-test is performed to evaluate the statistic significance of each regressor, and a p-value threshold is used to select the most meaningful regressors as inputs of the black-box model. By doing so, the final model was obtained as

$$L_{est}(R_a) = \alpha_1 \sqrt[3]{R_a} + \alpha_0, \qquad (9)$$

whose identification results are shown in the right plot of Fig. 3, showing a good fitting of the measured data.

The same approach was followed to identify the relationship between R_g and the load distribution. Simulation tests was performed varying the front axle distribution from 40% to 60%, yielding the following model

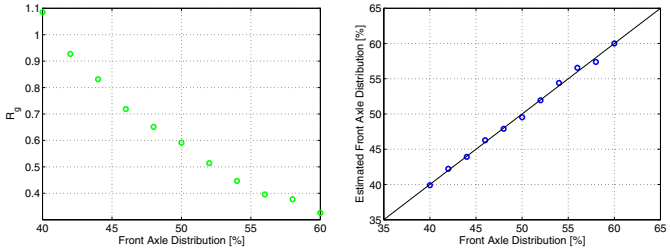

Fig. 4. Estimation of the load distribution: ratio index of the pitch rate spectrum (left); model fitting (right).

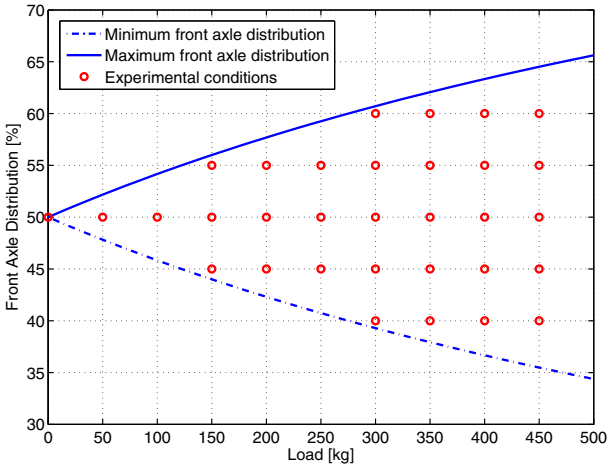

Fig. 5. Identification experiment: explored conditions.

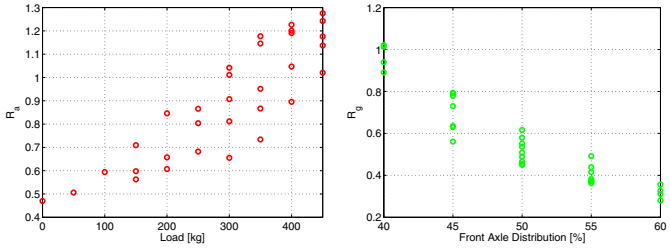

Fig. 6. Ratio index of the acceleration signal (left); ratio index of the pitch rage signal (right).

$$D_{est}(R_g) = \beta_2 \sqrt[3]{R_g} + \beta_1 \sqrt{R_g} + \beta_0. \tag{10}$$

The left plot of Fig. 4 shows the values of R_g, while the results of the load distribution model identification are represented in the right plot of Fig. 4, showing again good fitting performance.

Finally, a complete test in which both the load and the load distribution were varied was performed. As the load distribution is computed according to (3), not all combinations of load and load distribution are feasible. In Fig. 5, the simulated conditions are represented (load from 0 to 450 kg, distribution from 40% to 60%). The identified models are of the form

$$\begin{cases} L_{est}(R_a, R_g) = \alpha'_4 \sqrt[3]{R_a} + \alpha'_3 \sqrt[3]{R_g} + \alpha'_2 \sqrt{R_a} + \alpha'_1 R_a R_g + \alpha'_0 \\ D_{est}(R_a, R_g) = \beta'_3 \sqrt[3]{R_g} + \beta'_2 R_g + \beta'_1 {R_a}^2 + \beta'_0, \end{cases} \tag{11}$$

while the values of the ratio indexes and the identification results are shown in Fig. 6 and Fig. 7.

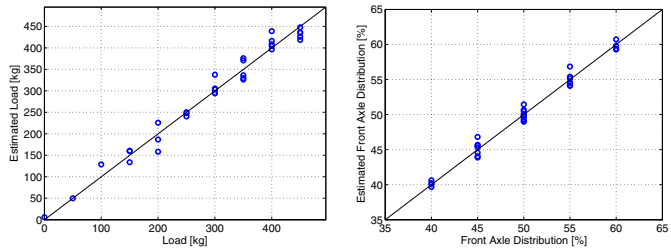

Fig. 7. Results of: load estimation (left); estimation of the load distribution (right).

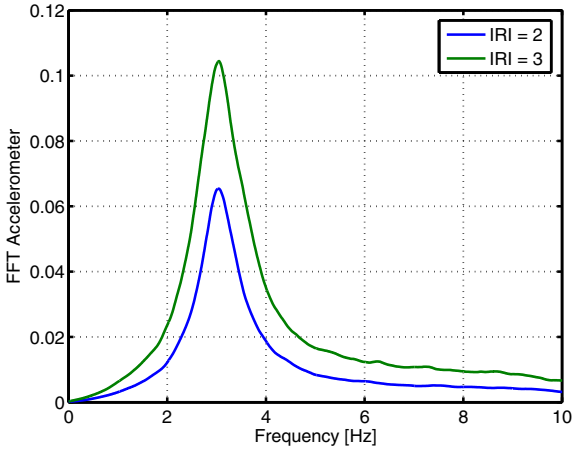

Fig. 8. Accelerometer spectra for two different IRI values.

3.3 Sensitivity analysis

Given the varied working conditions which a vehicle can be subject to, it is important to perform a sensitivity analysis of the ratio indexes R_a and R_g for different road profiles, and different values of the forward speed.

As discussed in Section 2, the road roughness is defined by the parameter σ^2 in (1), which acts as a gain on the amplitude of z_r. Of course, if the linear approximation of the vehicle dynamics of interest holds, the spectra of the two signals should not show variations in the frequency bands of interest if the road condition varies. Figure 8 confirms this assumption, showing that, actually, the variation of the road profile causes only a variation in the magnitude of the accelerometer spectrum, but no frequency shift of the abscissa of the maximum. As such, given that such a variation appears, identical both at the numerator and at the denominator of the cost functions (7) and (8), there are no modifications of the cost functions. Similar results were obtained for the pitch rate signal.

Turning now to the vehicle speed, note that (1) shows that this variable has a direct impact on the low pass filter pole which determines the road profile signal z_r. In Fig. 9, the magnitude Bode plot of the frequency response associated to the transfer function of $\frac{1}{s+\alpha_r v}$ is represented, for different v (α_r = 0.15 in this case).

As a matter of fact, beyond a certain frequency f_{min} the influence of v on the spectra of interest can be considered as a pure magnitude variation acting on the road profile signal. If the vehicle is driven at a maximum speed of 150 km/h (higher than most of the existing speed limits on highways) f_{min} can be set at approximately 1.7 Hz. Thus, as all the band pass filters

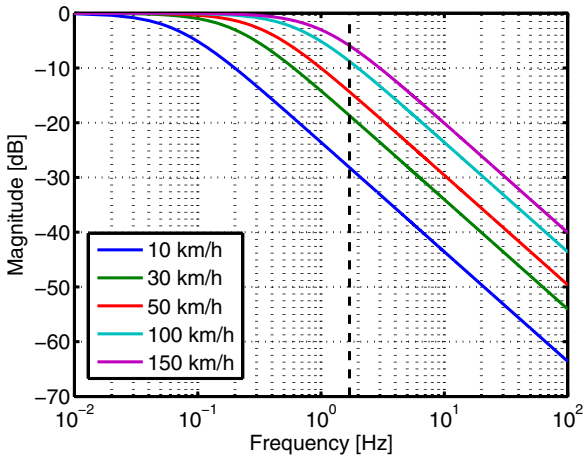

Fig. 9. Magnitude of the Bode plots associated to the road shaping filter for different speed values.

defined in Section 2.2 operate at frequency higher than f_{min}, the vehicle speed has no influence on the ratio index, as it only acts as a scaling factors on the spectra.

4. PERFORMANCE ANALYSIS AND VALIDATION

In this section, simulation tests will be performed in order to assess the estimation performance in a realistic situation. Further, experiments on the test vehicle will be also carried out to validate the whole approach. Particular attention will be paid to the accuracy of the estimation, and to the practical implementation of the method.

4.1 Simulation results

Within the CarSim simulation environment, three different type of test were considered: (i) Step variation of the vehicle load; (ii) Step variation of the vehicle load distribution; (iii) Random variations of both load and load distribution. In the first test the front axle load distribution is kept constant and equal to 50%, while the load is varied with a single step from 0 to 300kg. Conversely, in the second test load will be fixed and equal to 400kg, while the distribution will vary from 40% to 60%. Finally, in the last test random values of load and load distribution will be chosen among the feasible couples defined in Fig. 5. For all tests, the a road with IRI=4 was employed, and the vehicle was driven at 50km/h.

To be closer to the final implementation, an on line version of the estimation algorithm must be devised. Of course, being it based on the evaluation of the spectrum of the two signals of interest, batch of data must be stored for data processing. Specifically, data are recorded while the vehicle is running, and every N minutes the algorithm is run on the last batch of data. In the following simulations, batches of 5 minutes were analyzed with data sampled at 50 Hz. The values of the mean and the variance of the percentage error of the load estimation($\%Err_L$) and the load distribution estimation ($\%Err_D$) will be given as indications of the estimation accuracy. The percentage error is computed as

$$\%Err_L = \left| \frac{L_{est} - L}{L_{max} - L_{min}} \right|$$
$$\%Err_D = \left| \frac{D_{est} - D}{D_{max} - D_{min}} \right|, \qquad (12)$$

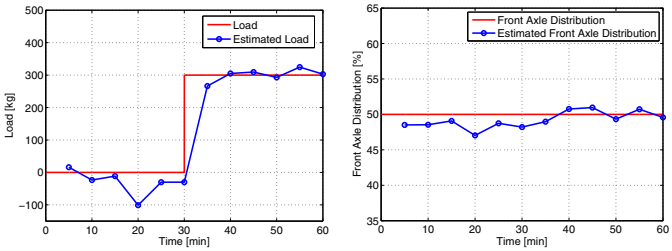

Fig. 10. Simulation results for test 1): Load estimation (left); Estimation of the load distribution (right).

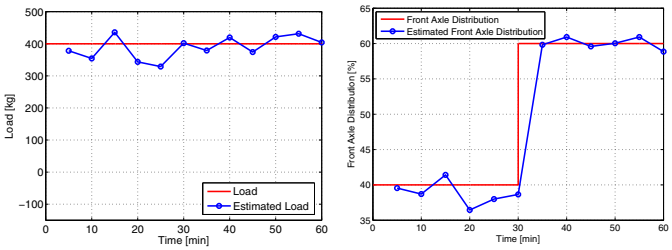

Fig. 11. Simulation results for test 2): Load estimation (left); Estimation of the load distribution (right).

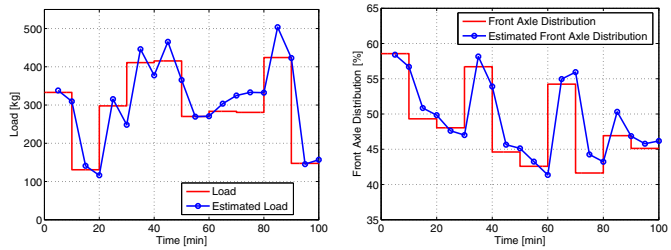

Fig. 12. Simulation results for test 3): Load estimation (left); Estimation of the load distribution (right).

where $L_{min} = 0$, $L_{max} = 450$, $D_{min} = 40$ and $D_{max} = 60$.

In Fig. 10, the results of the first simulation are shown. The complete model developed in (11) was used for the estimation. The values of the mean and the variance of the percentage error of the load estimation are the following: $\overline{\%Err_L}$=5.46%, $Var(\%Err_L)$=0.34%, $\overline{\%Err_D}$=6.02% and $Var(\%Err_D)$=0.12%, which show that a good accuracy in the load estimation is achieved.

Fig. 11 shows the results of the second test. In this case, the load distribution was shifted from 40% to 60% after 30 minutes from the beginning of the simulation. The overall results are: $\overline{\%Err_L}$=6.59%, $Var(\%Err_L)$=0.2%, $\overline{\%Err_D}$=5.69% and $Var(\%Err_D)$=0.23%, showing again good estimation performance.

Finally, in Fig. 12 the results of the third validation test are displayed. Ten random values of load and load distribution were chosen among the feasible ones defined in Fig. 5, and each of them was kept fixed for 10 minutes.

The overall percentage errors were: $\overline{\%Err_L}$=6.08%, $Var(\%Err_L)$ =0.26%, $\overline{\%Err_D}$=6.25% and $Var(\%Err_D)$=0.2%, thus proving the effectiveness of the approach also in a more challenging test with several variations in both load and its distribution.

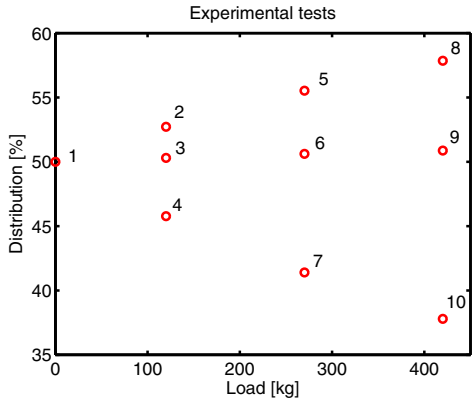

Fig. 13. Working conditions explored in the experimental setting.

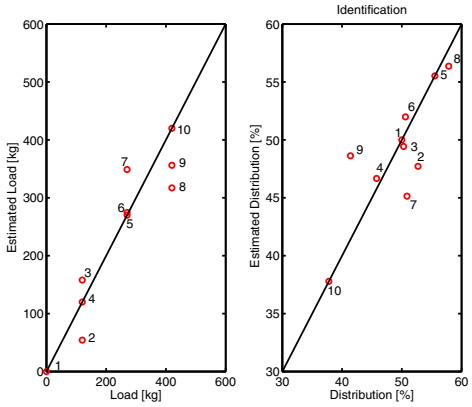

Fig. 14. Results of the identification experiments: estimation of the load (left) and of the load distribution (right).

4.2 Experimental results

Let us now consider the experimental results obtained on the small van used as test vehicle. The experimental conditions spanned in the tests are shown in Fig. 13, where the pairs of load and load distribution considered in the experiments are displayed. Specifically, the working conditions are as follows: (i) Different vehicle loads, with values (0, 120, 270, 420)kg; (ii) Different load distributions, realized by concentrating the load in the front, middle and rear part of trunk, respectively. These positions correspond approximately to $d = 0.5, 1.3, 2.8$ with $l = 2.8$ m (see (3)). All data was measured during tests carried out on a dry urban asphalt road, with a vehicle speed of approximately 50 km/h. Each test was approximately 15 minutes long, and data was sampled at 50 Hz. For analysis purposes, the data measured in each test was divided into identification and validation data sets (specifically, 2/3 of the test was used for identification and 1/3 for validation).

The results obtained in the identification experiments are shown in Fig. 14, both for the load estimation (left plot) and for the estimation of the load distribution (right plot). The numbers associated with each data point allows one to map them onto the test grid shown in Figure 13. These experiments were used to tune the parameters of models (11) to the measured data, without modifying the model structure. As can be seen, the performance degradation moving to an experimental setting is quite limited, and the performance remains satisfactory, as confirmed by the quantitative results: in fact, $\overline{\%Err_L}$=7.87%, $\overline{\%Err_D}$=11.28%, $Var(\%Err_D)$=13.41%. Using the validation data, the following performance was obtained: $\overline{\%Err_L}$=8.98%, $Var(\%Err_L)$=4.81%, $\overline{\%Err_D}$=20.55% and $Var(\%Err_D)$=13.58%. A quite limited degradation with respect to the identification case is observed, which proves the robustness of the proposed method.

5. CONCLUDING REMARKS

This paper presented a frequency-based data processing method for the estimation of the vehicle load and of its distribution inside the trunk of a vehicle. The approach is based on the spectral analysis of the vertical accelerometer and the pitch gyroscope signals, which are low-cost sensors that can be very easily installed on board if not yet present in the vehicle instrumentation. The effectiveness of the proposed estimation method was assessed both via simulations in the CarSim environment and on experimental data measured on a small van.

REFERENCES

H.K. Fathy, D. Kang, and J.L. Stein. Online vehicle mass estimation using recursive least squares and supervisory data extraction. In *American Control Conference, 2008*, pages 1842–1848, 2008.

H. Imine, V. Dolcemascolo, and B. Jacob. Wheel and heavy vehicle load estimation using road profile. In *Proceedings of the 9th International Symposium On Heavy Vehicle Weights And Dimensions, ISHVWD'09*, 2006.

J.A. at al. Lacuck. Vehicle load measuring apparatus, 1971. US Patent 3,603,418.

W.D.O. Paterson. International roughness index: Relationship to other measures of roughness and riding quality. *Transportation Research Record*, (1084), 1986.

B.L. Pence. *Recursive parameter estimation using polynomial chaos theory applied to vehicle mass estimation for rough terrain*. PhD thesis, Pennsylvania State University, 2011.

K.W. Reichow, D.C. English, and J.L. McCauley. Vehicle load measuring system, 1977. US Patent 4,042,049.

R.W. Rotenberg. Vehicle suspension. *Mashinostroenie, Moscow*, 1972.

M. Rozyn and N. Zhang. A method for estimation of vehicle inertial parameters. *Vehicle system dynamics*, 48(5):547–565, 2010.

S.M. Savaresi, S. Bottelli, M. Tanelli, and I. Boniolo. System and method for the estimation of one or more parameters related to the load of a vehicle, specifically of its absolute value and its distribution, 2013. Italian Patent MI2013A000802, filed on 16/05/2013. Applicants: Politecnico di Milano, E-NOVIA s.r.l.

G. Stefansson and K. Lumsden. Performance issues of smart transportation management systems. *International Journal of Productivity and Performance Management*, 58(1):55–70, 2008.

A. Vahidi, A. Stefanopoulou, and H. Peng. Recursive least squares with forgetting for online estimation of vehicle mass and road grade: theory and experiments. *Vehicle System Dynamics*, 43(1):31–55, 2005.

V. Winstead and I.V. Kolmanovsky. Estimation of road grade and vehicle mass via model predictive control. In *Proceedings of 2005 IEEE Conference on Control Applications, 2005*, pages 1588–1593, 2005.